Journal of Statistical Physics, Vol. 52, Nos. 1/2, 1988

Simulation of Wetting and Drying at Solid–Fluid Interfaces on the Delft Molecular Dynamics Processor

J. H. Sikkenk,[1] J. O. Indekeu,[1,2] J. M. J. van Leeuwen,[1] E. O. Vossnack,[3] and A. F. Bakker[3]

Received September 3, 1987; revision received March 1, 1988

The adsorption is studied of a fluid at a structured solid substrate by means of computer simulations on the Delft Molecular Dynamics Processor. Two types of particles are present, 2904 of one type for building a three-layer substrate and about 8500 of another type for composing the fluid. Interactions between like and unlike atoms are modeled by pair potentials of Lennard-Jones form cut off at 2.5σ. Simulations are performed at constant temperature and variable ratio of substrate–adsorbate to adsorbate–adsorbate attraction. On the basis of measurements of density profiles, coverages, surface tensions, and contact angles, a wetting as well as a drying phase transition have been identified. Both transitions are of first order.

KEY WORDS: Wetting and drying phase transition; molecular dynamics simulation; contact angle; surface tension; adsorption; special-purpose computer.

1. INTRODUCTION

Since the theoretical discovery of the wetting phase transition in 1977 by Cahn[1] and Ebner and Saam[2] and its experimental confirmation in 1980 by Moldover and Cahn,[3] many statistical mechanical models[4] and theories featuring density functionals[5] have displayed a phase transition from partial to complete wetting. Several experiments have shown a

[1] Instituut Lorentz, Rijksuniversiteit Leiden, Leiden, The Netherlands.
[2] Present address: Molecular Physics Laboratory, Katholieke Universiteit Leuven, 3030 Leuven, Belgium.
[3] Laboratorium voor Technische Natuurkunde, Technische Universiteit Delft, 2600 GA Delft, The Netherlands.

0022-4715/88/0700-0023$06.00/0

wetting transition (see ref. 6 for review) and many have studied the question of incomplete or complete wetting (e.g., ref. 7) and discussed the thickness of wetting layers.[8]

It has often been argued on the basis of scaling theory that a wetting (or drying) phase transition is unavoidable and ubiquitous near a critical point. However, scaling arguments alone are inconclusive as far as the necessity of the transition is concerned,[9] even in systems with only short-range forces.[10] Theoretical and experimental cases have been found where the transition does not occur (neither wetting nor the complementary phenomenon of drying).[9–13] As far as we know, systems without a wetting transition involve a subtle interplay between short-range (e.g., exponential decay) and long-range (power-law decay) forces.

On the basis of the evidence gathered so far it is reasonable to conclude that the existence and the nature (first- or second-order character) of a wetting or drying transition are far from universal. They sensitively depend on microscopic details of interfaces (e.g., chemical structure of substrate–asorbate interface) and on the details (in particular, the range) of the direct interactions (resulting from intermolecular forces) and the fluctuation-induced interactions between interfaces (see ref. 14 for a recent review).

As an important bridge between theoretical and experimental approaches, computer simulations can complement our understanding of wetting phenomena. Modern computational statistical mechanics makes use of (super) computers[15] and special-purpose computers[16] in an attempt to simulate systems—in our case continuum fluids—in a highly realistic fashion. In this paper we present the details of our previously reported simulations.[17]

2. DESCRIPTION OF THE SYSTEM

Computer simulations of the wetting transition are difficult because one needs a large system to accommodate the various phases (substrate, liquid, and vapor) and consequently the system equilibrates slowly near the phase transition. In lattice gases (Ising models) Monte Carlo simulations of the wetting problem have been quite successful.[18] In fluids with continuous degrees of freedom simulations are harder to perform. Previous molecular dynamics simulations of adsorption dealt with numbers of particles ranging between 200 and 1200.[19,20] The influence of a structured wall on an adjacent fluid has also been investigated by Abraham by means of Monte Carlo simulations.[21] In all cases the interaction with the substrate was represented by external potentials.

We report on simulations using the Delft Molecular Dynamics Processor[22] with two types of atoms, 2904 of one type for building a solid substrate and about 8500 of the other type for composing the fluid adsorbate. All pairs of atoms i and j interact with Lennard-Jones potentials ϕ_{AB}, where A or B are replaced by s for atoms in the solid and by f for atoms in the fluid. We have

$$\phi_{AB}(r_{ij}) = 4\varepsilon_{AB}[(\sigma_{AB}/r_{ij})^{12} - (\sigma_{AB}/r_{ij})^{6}] \tag{2.1}$$

where $r_{ij} = |r_i - r_j|$. All pair potentials are cut off at $2.5\sigma_{AB}$. As a consequence, we are dealing with *short-range interactions* only.

The solid substrate is structured. We took $\varepsilon_{ss} = 50\varepsilon_{ff}$ in order to build a stable, close-packed fcc solid substrate of three layers. The layers belong to (100) planes of the solid and the first and the third layers form the surfaces of the substrate. Particles in the solid are three times more massive than in the fluid ($m_s = 3m_f$). Therefore, apart from small vibrations, the substrate is rigid. The lattice spacing, dictated by $\sigma_{ss} = 0.847\sigma_{ff}$, is chosen such that there is a mismatch between solid and fluid. This prevents solidification of the first adsorbed liquid layers. The interaction between substrate and adsorbate is further characterized by $\sigma_{sf} = 0.912\sigma_{ff}$. This particular proportionality factor has been chosen close to the mean of σ_{ss} and σ_{ff}. The cubic box in which the fluid and the substrate reside has linear size $L = 29.1\sigma_{ff}$ and the boundary conditions are periodic in all three dimensions. Note that adsorption takes place on either side of the three-layer substrate. Because of the potential cutoff, adsorbed atoms on one side are strictly outside the interaction range of adsorbed atoms on the other side.

Denote the total free energy of the system by

$$F = -k_B T \log Z \tag{2.2}$$

where Z is the canonical partition function. The total surface tension of the system s_{tot} is then defined as

$$s_{\text{tot}} = \left(\frac{\partial F}{\partial \mathscr{A}}\right)_{T,V,N_s,N_f} \tag{2.3}$$

where $\mathscr{A}$ is the substrate area. Temperature T, volume V, and numbers of atoms in the solid N_s and in the fluid N_f are fixed. After differentiation one obtains[23]

$$s_{\text{tot}} = \left\langle \sum_{A,B} \sum_{i<j} \frac{d\phi_{AB}(r_{ij})}{dr_{ij}} \frac{(x_{ij}^2 + y_{ij}^2 - 2z_{ij}^2)}{r_{ij}} \right\rangle \Big/ 2\mathscr{A} \tag{2.4}$$

where $\langle \cdots \rangle$ denotes the thermal average.

This result is equivalent to the mechanical definition of the surface tension as the integral around the (periodic) system of the difference of transverse and normal components (with respect to the substrate) of the pressure tensor[24]:

$$s_{\text{tot}} = \int_{-L/2}^{L/2} dz\, [p_N(z) - p_T(z)] \tag{2.5}$$

where z is the coordinate perpendicular to the substrate. We have assumed equivalence of x and y directions. In a bulk phase the difference $p_N - p_T$ vanishes and no contribution to the surface tension is made. In principle, this allows the separation of s_{tot} into the different surface tensions s_{sv}, s_{sl}, and s_{lv} (where the subscripts s, l, and v denote solid, liquid, and vapor, respectively).

Next we define the total surface free energy γ_{tot} through the following expression for F:

$$F = \sum_i V_i f_i + \sum_i \mu_i \Gamma_i + \mathscr{A}\gamma_{\text{tot}} \tag{2.6}$$

where f_i denotes the bulk free energy density, V_i the volume, μ_i the chemical potential, and Γ_i the coverage associated with phase i. The surface free energy γ_{tot} is thus independent of the choice of dividing surfaces. When appropriate Gibbs dividing surfaces are chosen to separate adjacent phases, the term $\sum_i \mu_i \Gamma_i$ vanishes.[24] The relation between s_{tot} and γ_{tot} is

$$s_{\text{tot}} = \partial F/\partial \mathscr{A} = \gamma_{\text{tot}} + \mathscr{A}\, \partial\gamma_{\text{tot}}/\partial \mathscr{A} \tag{2.7}$$

The relevant quantity in the thermodynamics of wetting and drying is γ_{tot}.[25] For the liquid–vapor interface $s_{lv} = \gamma_{lv}$ because γ_{lv} is insensitive to the surface area. For the interfaces involving solid walls the surface free energy is sensitive to the area per atom because a solid can support stress. One of the problems in our simulations is that we are able to compute s_{tot} [using (2.4) or (2.5)], but not γ_{tot}. We will come back to this problem in detail in the discussion (Section 5). Another problem is the separation of s_{tot} into s_{sl}, s_{sv} and s_{lv}. Note that these tensions are well defined only if one can integrate (2.5) from inside a bulk phase (where $p_N = p_T$) to another bulk phase. For the determination of γ_{lv} we have generally sufficiently large bulk phases on either side of the liquid–vapor interface such that the interfacial tension can be calculated uniquely. Since our solid consists of only three layers, which are in general also subject to lateral stresses (e.g., due to periodic boundary conditions), we do not expect $p_T = p_N$ inside the substrate. We have tried to minimize the influence of stresses as follows. We

have investigated solid walls of 3, 5, 7, and 9 layers surrounded by vacuum and adjusted the system size L such that the central layer achieved the condition of isotropic pressure. For walls of 7 and 9 layers the values of L so obtained are almost identical, and we have adopted this system size for our three-layer wall. In our opinion this situation comes closest to the stresses experienced by the surface layers of a bulk solid that is free from stresses in its interior.

3. THERMODYNAMICS OF WETTING AND DRYING: PROFILE SYMMETRIES

The evidence for the occurrence of wetting or drying transitions in computer simulation of fluids has been rather limited up to now. Van Swol and Henderson[20] located in their system of 512 particles interacting with square-well potentials a drying transition on the basis of an examination of density profiles and coverages in addition to an analysis of surface free energy data, with the help of statistical sum rules. In their system, the statistical sum rules can be worked out to yield practical equations because of the piecewise-constant potentials (square wells). In Section 5 we discuss the relationship between their results and ours.

We briefly review some basic thermodynamic relations. The condition of thermodynamic stability

$$\gamma_{sv} \leqslant \gamma_{sl} + \gamma_{lv} \tag{3.1}$$

expresses that a solid–vapor interface with surface free energy γ_{sv} is thermodynamically stable as long as the inequality is strictly satisfied. In this case the solid is incompletely wet (assuming that the solid preferentially adsorbs the liquid phase, i.e., $\gamma_{sl} < \gamma_{sv}$). If the equality is realized, the stable profile consists of a solid–liquid interface with surface free energy γ_{sl} combined with a liquid–vapor interface with surface free energy γ_{lv} at a macroscopic distance away from the solid surface. The solid is then completely wet. Analogously,

$$\gamma_{sl} \leqslant \gamma_{sv} + \gamma_{lv} \tag{3.2}$$

expresses incomplete ($<$) or complete ($=$) drying of the solid. For incomplete wetting or drying, the contact angle Θ is defined by

$$\gamma_{lv} \cos \Theta \equiv \gamma_{sv} - \gamma_{sl} \tag{3.3}$$

expressing mechanical equilibrium of the three-phase contact line (Young's law).

Our simulations are done in the canonical ensemble. The number of atoms in the solid N_s as well as in the fluid N_f are fixed. It is then possible to enforce liquid–vapor coexistence by adjusting N_f such that at least one liquid–vapor interface is maintained in the system. At a given temperature, we thus obtain the pressure corresponding to phase coexistence in bulk.

Density profiles (density versus z) can consist of two solid–liquid interfaces and two liquid–vapor interfaces bounding a vapor phase in the middle (Fig. 1). They can also be composed of two solid–vapor interfaces and two liquid–vapor interfaces bounding a liquid (Fig. 2). These profiles are *symmetric*: the coverage (the integral along z of the excess density of adsorbate relative to bulk density) is the same on both sides of the substrate. Although both sides of the substrate are identical, *asymmetric* profiles also occur. They contain one solid–vapor, one solid–liquid, and one liquid–vapor interface (Fig. 3).

The symmetric profiles correspond to a total surface free energy

$$\gamma_{\text{tot}} = 2\gamma_{sl} + 2\gamma_{lv} \qquad \text{(Fig. 1)} \tag{3.4}$$

or

$$\gamma_{\text{tot}} = 2\gamma_{sv} + 2\gamma_{lv} \qquad \text{(Fig. 2)} \tag{3.5}$$

The asymmetric profile has

$$\gamma_{\text{tot}} = \gamma_{sl} + \gamma_{sv} + \gamma_{lv} \qquad \text{(Fig. 3)} \tag{3.6}$$

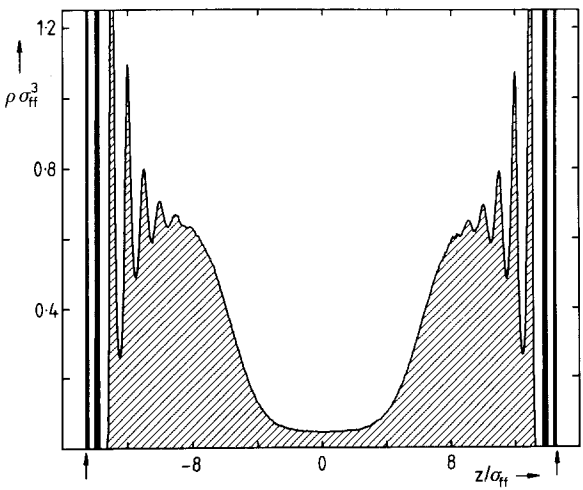

Fig. 1. Density profile of a symmetric (completely wet) configuration at $\varepsilon_r = 0.85$, averaged over a trajectory of 5.2×10^4 consecutive time steps. Dark peaks correspond to the substrate layers. The arrows denote the periodic boundary.

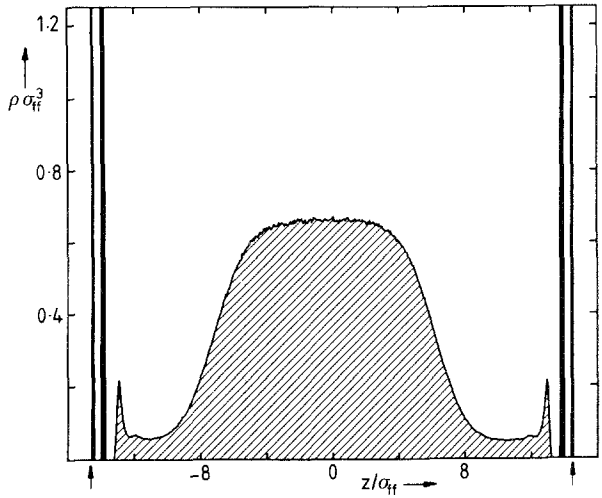

Fig. 2. Density profile of a symmetric (completely dry) configuration at $\varepsilon_r = 0.3$, averaged over a trajectory of 2.6×10^4 consecutive time steps.

For studying the wetting or drying phase transitions one can vary the temperature at liquid–vapor coexistence. The transition is expected when the temperature is increased toward the critical temperature of the fluid.[1–6] In the case of wetting, an adsorbed liquid film of *microscopic* thickness grows suddenly into a layer of *macroscopic* thickness. For drying, the

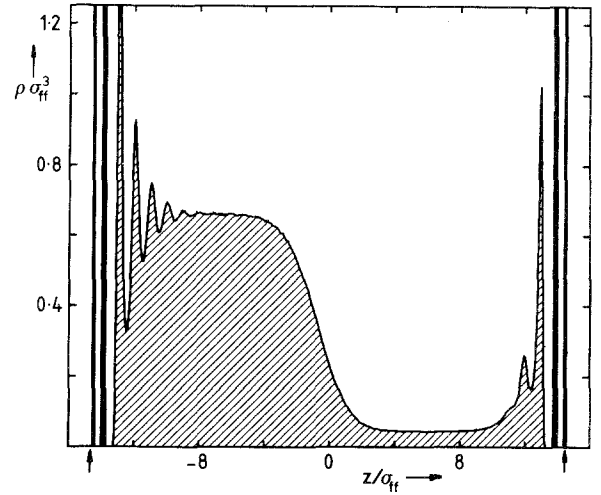

Fig. 3. Density profile of an asymmetric configuration at $\varepsilon_r = 0.65$, averaged over a trajectory of 5.2×10^4 consecutive time steps.

adsorbed phase is a vapor. The principal variables for discussing these phase transitions are temperature and surface field.[26] In the case of wetting one can make the transition from the incompletely wet phase to the completely wet phase either by raising the temperature or by increasing the preference of the solid for adsorption of the liquid phase. The latter possibility corresponds to increasing the surface field, which in our system is represented by the ratio $\varepsilon_r \equiv \varepsilon_{sf}/\varepsilon_{ff}$ of the Lennard-Jones parameters. Remark that one may treat ε_r as an independent variable, keeping ε_{ss} and ε_{ff} fixed. This feature is also exploited in experiments where one chemically alters the outermost layers, thereby modifying the local solid–fluid interactions.[12]

In our simulations it is convenient to study wetting at fixed temperature and varying ε_r, because then the coexisting bulk densities ρ_l and ρ_v and also the surface tension of the liquid–vapor interface γ_{lv} are fixed, and only the coverages and the substrate–fluid surface tensions vary. Under these circumstances the thermodynamically stable profile that minimizes γ_{tot} can have different symmetry. If surface phase transitions take place, singularities occur in the minimal total surface free energy as a function of ε_r. In the case of a first-order phase transition the derivative of this function is discontinuous and metastable continuations of stable profile symmetries are expected. From Eqs. (3.4)–(3.6) it follows directly that if a profile such as that in Fig. 1 is stable, the substrate is completely wet ($\Theta = 0$). Indeed, if γ_{tot} as given by (3.4) is lower than the values of γ_{tot} in (3.5) and (3.6), then a direct solid–vapor contact is not possible in equilibrium because its surface free energy γ_{sv} would exceed the sum $\gamma_{sl} + \gamma_{lv}$. Analogously, the substrate is completely dry ($\Theta = \pi$) if the stable profile has the form of that in Fig. 2. Finally, the stability of an asymmetric profile (Fig. 3) implies incomplete wetting or drying ($0 < \Theta < \pi$).

4. RESULTS FROM THE SIMULATIONS

The speed of the special-purpose computer is comparable to that of a CRAY-1 supercomputer. Our simulations took a total of about 2000 of CPU time. We simulated the system at a fixed temperature $T^* = k_B T/\varepsilon_{ff} = 0.9$, which is between the triple temperature $T_t^* \simeq 0.7$ and the critical temperature $T_c^* \simeq 1.26$ of the bulk adsorbate. The temperature is kept constant by regularly adjusting the kinetic energy. This is done for the two types of atoms separately. At a given value of ε_r we allowed 1×10^4 time steps of $\Delta t^* = t/\sigma_{ff}(m_f/\varepsilon_{ff})^{1/2} = 0.01$ for equilibration. The initial configuration for a specific value of ε_r was taken to be an equilibrated configuration at a slightly different ε_r. The equilibration time was long enough to obtain stable bulk densities in liquid and vapor, total

energy, and coverages in most of the cases. After equilibration, measurements were made of pressure-tensor components[4] and density profile (every 13 time steps), and kinetic energy, potential energy, and pressure (every time step). To get a notion of statistical reliability, the runs were divided into subruns of 5200 time steps. Typically, runs took 5–20 subruns. Error bars in Figs. 7, 8, and 10 are based on results from these subruns.

At the first stage of our investigation we looked at density profiles and coverages between $\varepsilon_r \simeq 0.1$ and $\varepsilon_r \simeq 1.0$. The following qualitative picture emerges. At low ε_r symmetric (completely dry) profiles occur, and symmetric (completely wet) profiles are seen at high ε_r. In between, asymmetric profiles appear. There are large overlaps (intervals of ε_r values) where both symmetries are found.

To complement the information contained in the density profiles of Figs. 1–3, we visualized snapshots of particle configurations. For example, for an asymmetric profile we projected the positions of the centers of all atoms in the box onto a plane parallel to the xz plane. The result is shown in Fig. 4. We also represented the adsorption at the substrate surfaces by

[4] For special manipulation of the results obtained in the Delft Molecular Dynamics Processor, such as the computation of the pressure-tensor components and surface tensions, an array-processor (AP-120B) was used, which is attached directly to the special-purpose computer.

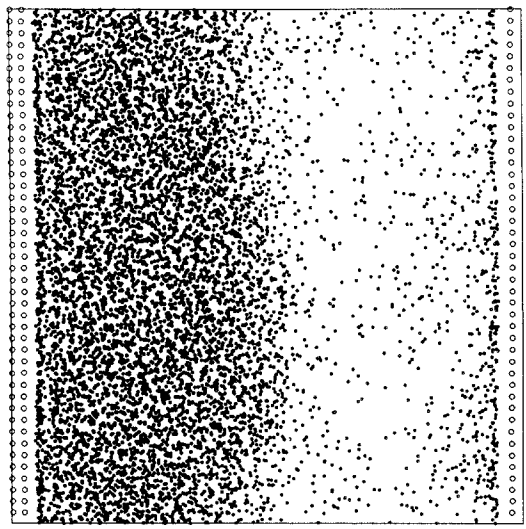

Fig. 4. The positions of the atoms projected on the xz plane for an asymmetric configuration with $\varepsilon_r = 0.65$. For clarity all z coordinates are shifted by a small amount with respect to the density profile in Fig. 3.

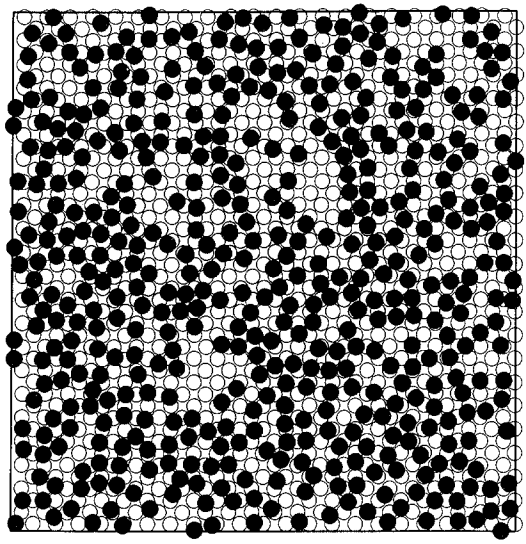

Fig. 5. The atoms in the first adsorbed layer at the solid–liquid interface (filled circles) together with the (100) substrate surface (open circles) at $\varepsilon_r = 0.65$.

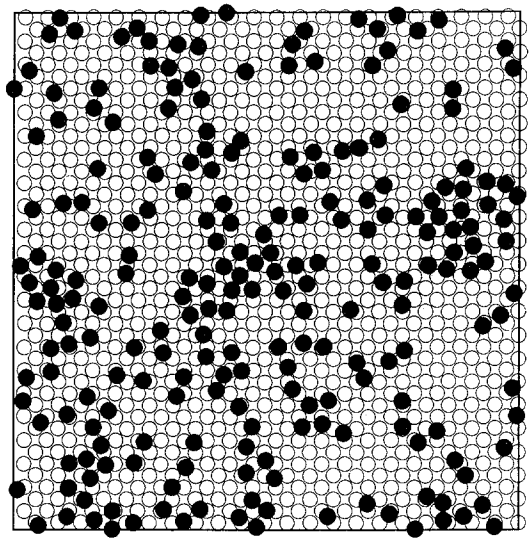

Fig. 6. The atoms in the first adsorbed layer at the solid–vapor interface (filled circles) together with the (100) substrate surface (open circles) at $\varepsilon_r = 0.65$.

taking a section of approximate width $2\sigma_{ff}$ parallel to the xy plane. This section includes the surface layer of the substrate and the first adsorbed atomic layer. The atoms are visualized as circles of approximate diameter σ_{ss} and σ_{ff}, respectively. Figure 5 shows the adsorption at the solid–liquid interface and Fig. 6 presents a view of the corresponding adsorption on the opposite surface of the substrate, at the solid–vapor interface. The densities of these first adsorbed layers correspond to the fluid density peaks in Fig. 3 closest to the substrate density peaks on the left and right, respectively.

Looking at the symmetric density profiles in Figs. 1 and 2, one can see that our box is not extended enough along the z direction to comfortably accommodate three bulk phases (liquids or vapors). This problem is inherent to the hardware structure of our computer.

Our second source of information is provided by data of the total surface tension s_{tot} as defined in Eq. (2.5). Figure 7 displays s_{tot} versus ε_r. The high values of s_{tot} found in our simulations are due to the strong forces between the solid particles, which we need in order to keep our three-layer solid stable ($\varepsilon_{ss} = 50\varepsilon_{ff}$). The major contribution to s_{tot} ($79.7\varepsilon_{ff}/\sigma_{ff}^2$) is already present in a solid–vacuum system and forms a constant background, which has no influence on quantities of relevance, such as the difference $s_{sv} - s_{sl}$. Data points with open circles refer to asymmetric profiles, and filled symbols (circles and squares) correspond to symmetric profiles. We distinguish three curves. First, a curve (open circles) between

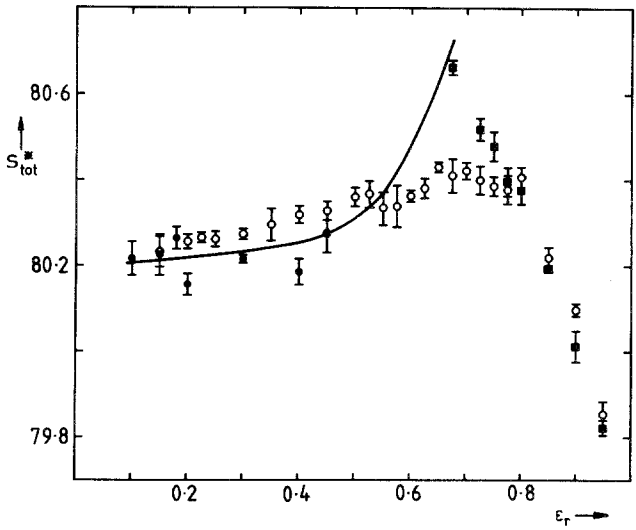

Fig. 7. The reduced total surface tension s^*_{tot} (in units of $\varepsilon_{ff}/\sigma_{ff}^2$) versus ε_r. (○) Asymmetric profiles, (■) completely wet substrates, (●) completely dry substrates. (—) Constructed from contact angle measurements.

$\varepsilon_r \simeq 0.1$ and $\varepsilon_r \simeq 0.8$, which is more or less a straight line, associated with asymmetric profiles. This curve meets a steep curve (filled squares) representing completely wet substrates at $\varepsilon_r \simeq 0.8$, and almost merges with the latter at higher ε_r. Assuming for the moment that γ_{tot} is quantitatively similar to s_{tot}, i.e., that the term $\partial\gamma/\partial\mathscr{A}$ in Eq. (2.7) plays no significant role, we see that below $\varepsilon_r = 0.78 \pm 0.03$ the incompletely wet substrate is the thermodynamically more stable configuration, whereas the completely wet substrate minimizes s_{tot} above this value of ε_r. The third curve (filled circles) consists of data points of completely dry substrates. Most of these data are based on relatively short observation times (about four subruns) and therefore less accurate. We further comment on these data in the next section. However, if the data are complemented with information from contact-angle measurements, the drawn curve results for the total surface tension of completely dry substrates. We see that below $\varepsilon_r = 0.54 \pm 0.03$ the completely dry substrate minimizes s_{tot}, whereas the incompletely dry substrate is the thermodynamically more stable configuration at higher ε_r (again assuming $\gamma_{\text{tot}} \simeq s_{\text{tot}}$).

The third route toward understanding the behavior of our system has been the determination of contact angles on the basis of surface tensions corresponding to the distinct interfaces in the system. This is easy whenever interfaces are separated by bulk phases where the integrand of Eq. (2.5) vanishes. In the cases of asymmetric profiles we have been able to measure accurately the liquid–vapor tension. We obtain $\gamma_{lv} = 0.22 \pm 0.01\varepsilon_{ff}^2$, independent of ε_r, as Fig. 8 shows. Moreover, this numerical value agrees with that obtained in a fully periodic liquid–vapor system without substrate. In that system $\gamma_{\text{tot}} = 2\gamma_{lv}$. Simulations were performed on our DMDP and, independently, on a mainframe IBM.[27]

Less straightforward is the determination of s_{sl} and s_{sv}, because the solid substrate is only three layers thick. To appreciate fully the difficulties involved in separating interfaces from bulk phases, we can examine the profile of the pressure-tensor component difference $p_N(z) - p_T(z)$, displayed in Fig. 9. This profile corresponds to the density profile of Fig. 3. We notice that only in the bulk vapor phase does $p_N(z) - p_T(z)$ have negligible fluctuations around zero. In the bulk liquid the fluctuations are significant, but fortunately yield zero average already over small intervals $\Delta z \lesssim \sigma_{ff}$. Therefore, γ_{lv} and also the *sum* $s_{sl} + s_{sv}$ can be accurately measured. The problem is to separate s_{sl} and s_{sv}. We have obtained an approximate separation as follows. Contributions to the integrand in Eq. (2.5) arising from the interactions of the substrate with the adsorbate on one side have been attributed to the interfacial tension on that side. Further, contributions arising from the solid–solid interactions within the second (central) substrate layer are divided equally over either side.

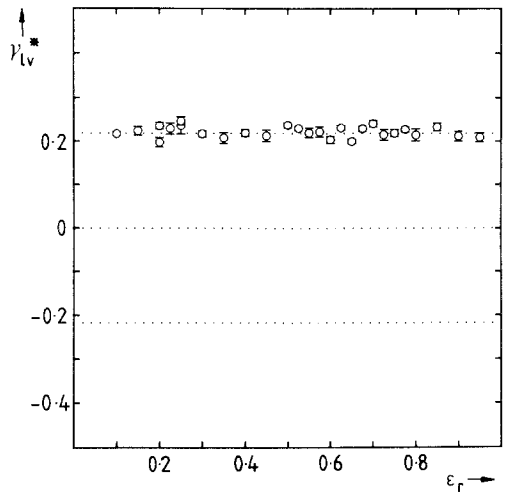

Fig. 8. The reduced surface tension γ_{lv}^* of the liquid–vapor interface (in units of $\varepsilon_{ff}/\sigma_{ff}^2$) versus ε_r.

Again assuming that the effect of $\partial\gamma/\partial\mathscr{A}$ terms can be neglected, Fig. 10 then shows $\cos\Theta$, as obtained from Eq. (3.3), for asymmetric profiles (open circles in Fig. 7). The data corresponding to incompletely dry or incompletely wet substrates follow a strikingly straight line. In accordance with Fig. 7, these data suggest that incompletely wet substrates are

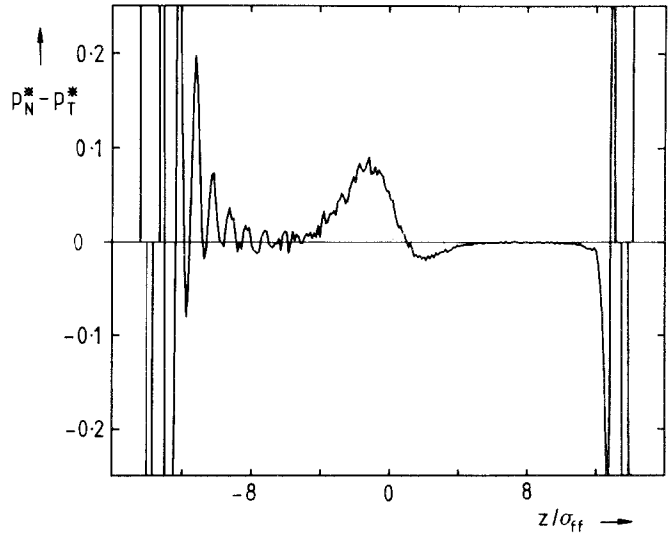

Fig. 9. The profile of the reduced difference $p_N(z) - p_T(z)$ (in units $\varepsilon_{ff}/\sigma_{ff}^3$) for $\varepsilon_r = 0.65$.

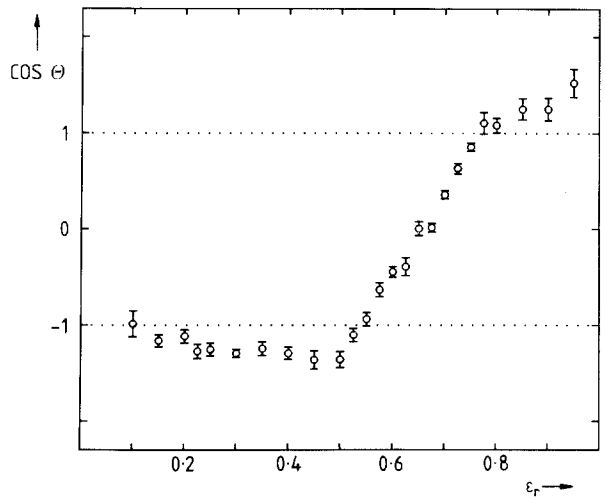

Fig. 10. The cosine of the contact angle Θ, obtained as $(s_{sv}-s_{sl})/\gamma_{lv}$, versus ε_r for asymmetric profiles ($-1<\cos\Theta<1$).

metastable for $\varepsilon_r \gtrsim 0.78$. Indeed, these states violate Eq. (3.1). Both the data of Fig. 7 and those of Fig. 10 locate the wetting transition at $\varepsilon_r = 0.78 \pm 0.03$. The consistency between total surface tension and contact-angle measurements relies particularly on the reliability of our approximate separation of s_{sl} and s_{sv}. This consistency thus suggests that we have accurately separated s_{sl} and s_{sv}, at least for ε_r around 0.8. At much lower ε_r, however, we can see in Fig. 7 that the data for completely dry substrates (filled circles) do not always fall on top of the solid line, where they should fall. The discrepancies, notably for $\varepsilon_r = 0.2$ and 0.4, may be due to the short observation times of completely dry states (affecting the data points), or perhaps also to inaccuracies in the separation of s_{sl} and s_{sv} (affecting the solid line). For the drying transition at $\varepsilon_r = 0.54$, however, we have only one independent location, namely, from the contact-angle measurements (Fig. 10). The solid curve drawn in Fig. 7 is constructed by summing $2(s_{sv}+\gamma_{lv})$, where s_{sv} and γ_{lv} are measured in the asymmetric profiles. The position of the drying transition determined from Fig. 7 is therefore necessarily consistent with the position that follows from the contact angle measurements. In the next section we discuss the time evolution of completely dry states at $\varepsilon_r \lesssim 0.54$ and examine the validity of the locations of the drying and wetting phase transitions at $\varepsilon_r \simeq 0.54$ and 0.78, respectively.

5. DISCUSSION

We first comment on the time evolution of density profiles of completely dry states. We have been able to observe completely dry states for a relatively short time only. Initially, the density profiles show dry walls and a bulk liquid in the middle of the system (e.g., Fig. 2). The position of the center of mass of the liquid droplet (or liquid film) can fluctuate in time due to velocity fluctuations inherent in our simulations. Indeed, the molecular dynamics is constrained by the requirement that the center of mass of all $N = N_s + N_f$ atoms be at rest. Relative motion of the substrate and the bulk liquid adsorbate can thus naturally occur, but can also be due to thermodynamic forces that equilibrate the system. For a whole range of values of ε_r, from as low as 0.1 up to 0.45, we have observed that the liquid droplet wanders away from the middle and collides with the substrate, typically after four subruns. At very low ε_r, e.g., 0.1, no real collision occurs, but the droplet gently touches the substrate. In spite of the very low value of ε_r, the droplet then stays at the substrate for a very long time (15 subruns), and subsequently leaves the substrate. This sequence of events is shown in Fig. 11. It appears quite evident to us that velocity fluctuations and not thermodynamic forces are responsible for this behavior, which resembles a random walk. We have performed this simulation with fewer adsorbate atoms than usual ($N_f = 5000$ instead of 8500) to allow a better accommodation of the vapor phases.

The situation becomes different at higher values of ε_r. At $\varepsilon_r = 0.2$, for example, the droplet moves to the substrate and then stays there for a time longer than we are able to measure. In fact, this is found for any $\varepsilon_r > 0.2$ as well. The collision between droplet and substrate becomes more dramatic as ε_r is increased. The time evolution at $\varepsilon_r = 0.4$ is shown in Fig. 12. The profile in Fig. 12d is qualitatively different from that in Fig. 12a. It looks as if a phase transition has taken place from a completely dry initial state to the partially dry state. Although we cannot rule out that the droplet may eventually leave the substrate again, there is some evidence that the behavior we see is mainly due to thermodynamic driving forces and that the stable state is partially dry. This evidence comes from the measurement of the internal energy U (per unit of area). In the course of the collision a "latent heat" of adsorption $\Delta U = -1.0\varepsilon_{ff}/\sigma_{ff}^2$ is absorbed by the heat bath. This is a large amount because typical fluctuations of the internal energy U over a subrun are one order of magnitude smaller.

Now we have a problem, because the surface-tension and contact-angle measurements indicate that the stable state at $\varepsilon_r = 0.4$ is completely dry. For example, from Fig. 7 one sees that the total surface tension of the partially dry state is higher than that of the completely dry state by an

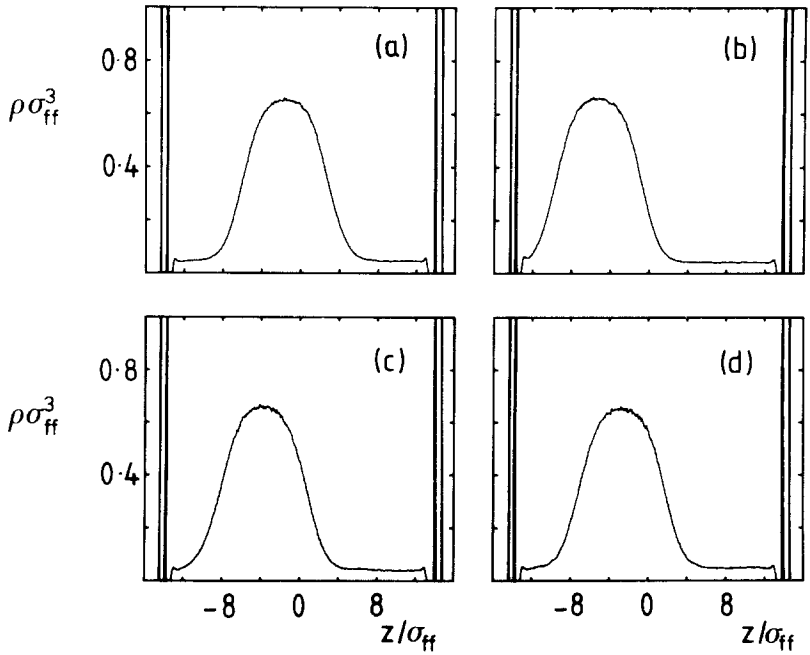

Fig. 11. Time evolution of a density profile at $\varepsilon_r = 0.1$. (a) After an initial motion to the right, the droplet turns to the left, and touches the substrate after four or five subruns; (b) The droplet stays near the surface for 15 subruns; (c) the droplet leaves the substrate and (d) moves to the center in five additional subruns.

amount $\Delta s_{\text{tot}} \simeq 0.1\varepsilon_{ff}/\sigma_{ff}^2$. For a range of values of ε_r below 0.54, the density profiles thus suggest that partial drying is stable, whereas the surface tensions indicate complete drying. Perhaps the most obvious explanation for this problem is that we have not measured the surface free energy γ, but the surface tension s, which includes the $\partial\gamma/\partial\mathscr{A}$ terms [see Eq. (2.7)]. For example, for obtaining the location of the drying transition we have imposed

$$\gamma_{sl} + \mathscr{A}(\partial\gamma/\partial\mathscr{A})_{sl} = \gamma_{sv} + \mathscr{A}(\partial\gamma/\partial\mathscr{A})_{sv} + \gamma_{lv} \tag{5.1}$$

When $\Delta\gamma = \mathscr{A}[(\partial\gamma/\partial\mathscr{A})_{sv} - (\partial\gamma/\partial\mathscr{A})_{sl}] \neq 0$ we have a shift in the drying point, which is likely toward smaller values of ε_r in view of the observed instability of the dry profiles, implying that $\Delta\gamma < 0$. Then $\Delta\gamma$ follows the difference in coverage Γ_1, which is the number of atoms adsorbed in the first layer on the substrate. In Fig. 13 we show the number of particles in the first adsorbed atomic layer for asymmetric profiles. The vertical lines mark the loci of the phase transitions that follow from Fig. 10. At $\varepsilon_r = 0.78$, where

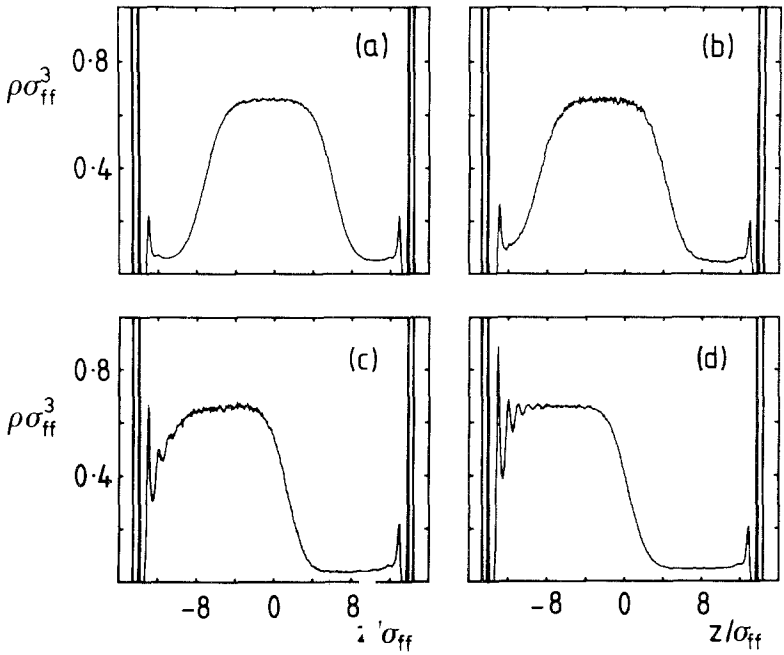

Fig. 12. Time evolution of a density profi. at $\varepsilon_r = 0.4$. (a) initially a droplet is near the center; (b) the droplet moves to the left (c) and reaches the substrate after four subruns; (d) configuration after ten additional subruns

the cos Θ plot locates the transition to complete wetting, the difference in the first-layer coverage of the solid–liquid and the solid–vapor interfaces is only small and we do not expect that $\Delta\gamma$ will change the location of the wetting transition very much. At $\varepsilon_r = 0.54$ the difference of the Γ_1 is quite large, and we can expect a larger correction to the value of cos Θ. Also for ε_r around 0.2 (and 0.9) we expect $\Delta\gamma \simeq 0$, and therefore conclude that the values of cos Θ for ε_r around 0.2 (and 0.9) are not affected. If $\Delta\gamma < 0$ for the relevant range of ε_r, the correct location of the drying transition must be somewhere between $\varepsilon_r = 0.2$ and $\varepsilon_r = 0.54$ and the wetting transition somewhat below $\varepsilon_r = 0.78$.

There are two other possible reasons that we can think of that might help explain why density profiles and surface tensions do not correspond well. One obvious reason is that we are not able to follow the system long enough and velocity fluctuations can easily be misinterpreted as thermodynamic driving forces. Second, even if we were sure to know the pertinent surface free energy, there would still be room for differences in the bulk contributions to the total free energy F between symmetric and asymmetric

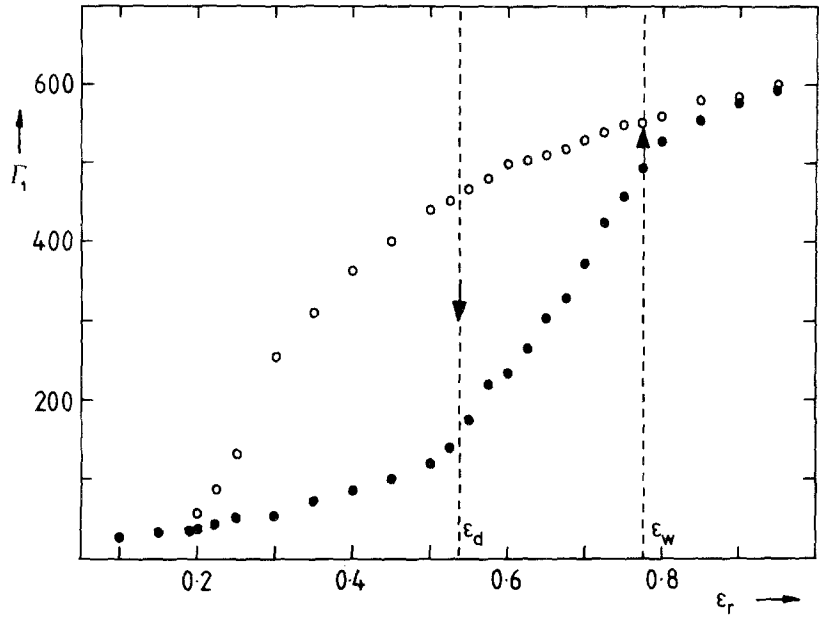

Fig. 13. The coverage Γ_1 in the first adsorbed atomic layer. (○) Γ_1 at the solid–liquid interface, (●) Γ_1 at the solid–vapor interface. Arrows denote the jumps in the coverage that would occur at the drying and wetting phase transitions determined by Fig. 10.

profiles. These differences may be present in view of the fact that bulk liquid and vapor phases are comfortably accommodated in an asymmetric profile, but much less so in symmetric profiles. In Fig. 1, for example, one sees that the bulk liquid density is nowhere well established, and a similar problem with the vapor density is apparent in Fig. 2. By contrast, there is no such problem with the profile of Fig. 3. Therefore, it is plausible that in our system of limited size an asymmetric profile is intrinsically more stable than a symmetric profile. This might reflect itself in a tendency for liquid droplets to attach easily to the substrate, in spite of a possible surface free energy barrier.

To conclude this part of the discussion, we note that if the difference $\gamma_{sv} - \gamma_{sl}$ depends on the area $\mathscr{A}$, such that it differs from our measured $s_{sv} - s_{sl}$, our cos Θ (as shown in Fig. 10) should also depend on the chosen value of $\mathscr{A}$. In our experiments $\mathscr{A}$ was taken such as to mimic best a stress-free bulk solid. For $\varepsilon_r = 0.4$ we varied $\mathscr{A}$ by 10%. Although the individual s_{sv} and s_{sl} change by a factor 5, the difference remains the same within the statistical error. This feature does not support our first explanation, but rather indicates that $\Delta\gamma \simeq 0$.

In the remainder of this section we attempt a comparison of the results obtained by van Swol and Henderson[20] with ours. Their simulations are based on a constant-temperature molecular dynamics procedure for a square-well fluid and are performed on 512-particle systems interacting via a $(\sigma, 3\sigma/2)$ square-well potential at a reduced temperature of $T^* = 1$, which is about half-way between the triple- and critical-point temperatures.

Their system is *asymmetric* in the z direction, consisting of one hard-wall boundary, which is necessarily always completely dry, and an opposite square-well wall, which can adsorb either vapor or liquid, depending on the depth of the well. In this way liquid–vapor coexistence is ensured. Only at the attracting wall can the density profile undergo a qualitative change. This happens at the drying transition. The wetting transition cannot be observed for their choice of walls, because incomplete wetting cannot be distinguished from complete wetting: in both cases the square-well wall is covered with a liquid phase and the hard wall by a vapor. This problem also makes it impossible to get hold of both γ_{sl} and γ_{sv} at the square-well wall simultaneously. Of course, they could easily have chosen a different system with two square-well walls and have studied the wetting transition.

An important difference in the geometry of the systems is that their box is rectangular and measures approximately $7 \times 7 \times 32$ (in units of σ_{ff} in each direction) along x, y, and z axes, respectively, whereas our box is cubic with sides of $29.1\sigma_{ff}$. Clearly, in our box the substrate area is 16 times larger and the number of adsorbate atoms is 16 times bigger as well, allowing substantial transverse fluctuations. Moreover, we have incorporated corrugation effects of a structured (and live) substrate. Together with the use of Lennard-Jones potentials, this has permitted us to obtain *realistic density profiles.*

In their simulations, van Swol and Henderson vary the ratio $\varepsilon_{\text{wall}}$ of the well depth of the wall–adsorbate potential and the well depth of the fluid–fluid potential. This $\varepsilon_{\text{wall}}$ corresponds qualitatively to our ratio ε_r of Lennard-Jones potential depths. A semiquantitative comparison is possible by remarking that in our Lennard-Jones system we can calculate an effective wall potential by integrating ϕ_{sf} over the substrate atoms. One obtains, in an approximation where the substrate is a homogeneous continuum,

$$\psi_{\text{eff}}(z) = \int_s d\mathbf{r}'\, \phi_{sf}(|\mathbf{r} - \mathbf{r}'|) n_s \tag{5.2}$$

where n_s is the number density of the fcc solid, which equals σ_{ss}^{-3} for nearest neighbor distances equal to $r_{\min}$, where $d\phi_{ss}(r_{\min})/dr = 0$. The result is

$$\psi_{\text{eff}}(z) = 4\pi \left(\frac{\sigma_{sf}}{\sigma_{ss}}\right)^3 \varepsilon_{sf} \left[\frac{1}{45}\left(\frac{\sigma_{sf}}{z}\right)^9 - \frac{1}{6}\left(\frac{\sigma_{sf}}{z}\right)^3\right] \tag{5.3}$$

The value of ψ_{eff} at its minimum equals

$$\psi_{\text{eff}}(z_{\min}) = -\frac{4}{9}\left(\frac{5}{2}\right)^{1/2} \pi \left(\frac{\sigma_{sf}}{\sigma_{ss}}\right)^3 \varepsilon_{sf} \equiv -\varepsilon_{\text{wall}}\varepsilon_{ff} \tag{5.4}$$

Therefore, $\varepsilon_{\text{wall}} \simeq 2.76\varepsilon_r$. We conclude that our drying and wetting transitions occur at $0.6 \simeq \varepsilon_{\text{wall}} \lesssim 1.5$ and $\varepsilon_{\text{wall}} \lesssim 2.2$, respectively. This agrees satisfactorily with the value found by van Swol and Henderson for the location of the drying transition, $0.85 \lesssim \varepsilon_{\text{wall}} \lesssim 1$, and with their extrapolations, which suggest a possible wetting transition at $\varepsilon_{\text{wall}} \simeq 2.1$.

An important question concerning the wetting and drying phase transitions is whether or not they are of first order. In the simulations by van Swol and Henderson the drying transition was claimed to be of first order,[20] but true hysteresis had not been observed.[20,28] In our simulation the most convincing evidence for the first-order character of the wetting and the drying phase transitions comes from the large hysteresis in the (symmetry of the) density profiles upon monotonically varying ε_r. The same hysteresis is also reflected in the intersections and metastable continuations of the branches of s_{tot} versus ε_r (Fig. 7). That we have included the $\partial\gamma/\partial\mathscr{A}$ terms in the surface free energy does not change these conclusions, because these terms can only quantitatively affect the curves in Figs. 7 and 10. The relevant qualitative features, such as the existence of metastable partially dry states for $\varepsilon_r \leqslant 0.2$ and metastable partially wet states for $\varepsilon_r \geqslant 0.9$, remain. Furthermore, we have correspondingly observed important hysteresis in the coverage and, in particular, in the number of particles Γ_1 in the first adsorbed atomic layer. This can be seen from Fig. 13. The jumps in Γ_1 associated with the phase transitions do not occur in the simulations. Instead, upon increasing or lowering ε_r, the coverages vary smoothly, as the data points indicate. Note that Γ_1 is not the order parameter associated with the surface phase transitions. The order parameter is the total coverage, a quantity that always remains finite in our canonical simulations but diverges at the transitions in a semi-infinite system.

To end of this section we make a general comment. As we have mentioned, we have dealt with short-range forces exclusively. The effects of the long-range tails of the van der Waals forces have been neglected altogether. These effects can in some instances change qualitatively the character of a wetting (or drying) transition. In general, second-order wetting transitions are turned into first-order ones and first-order transitions remain first order.[14] This would lead us to conclude that our picture would remain qualitatively valid. While this is expected to be true, it must be remarked that the numerical values of the interfacial tensions, e.g., of γ_{lv}, can change

significantly (by as much as 50% at temperatures not far above the triple point[29]). Therefore, we cannot exclude that the location of the phase transitions would be considerably altered.

In future simulations some topics in surface physics could be readily addressed with the present hardware. For example, the interesting problem of the adsorption of solids on solids can be studied. There, an important issue is the possible presence of strains in the adsorbed film, causing a mismatch between film and bulk adsorbate, and inhibiting the growth of a uniform macroscopic wetting layer. These strains can be reduced if the first adsorbed monolayer is rotated with respect to the symmetry direction of the substrate. This in turn depends on the ratio of σ_{ss} to σ_{ff}. In our simulations we have seen such rotation for large ε_r ($\varepsilon_{sf} \gg \varepsilon_{ff}$). Experimentally, such rotation has been seen, e.g., in Xe films on Pt (111).[30]

ACKNOWLEDGMENTS

We thank Dr. C. Bruin, Dr. R. Evans, Dr. D. Frenkel, M. Nijmeijer, and Prof. W. Van Dael for stimulating discussions. We are especially grateful to Dr. J. Henderson for sending unpublished details of simulations and for inspiring comments. We have benefited from a critical comment by F. van Swol. Part of this research was supported by the Stichting voor Fundamenteel Onderzoek de Materie, which is financially supported by the Nederlandse Organisatie voor Zuiver-Wetenschappelijk Onderzoek. One of us (J. O. I.) acknowledges support from the Belgian National Fund for Scientific Research.

REFERENCES

1. J. W. Cahn, *J. Chem. Phys.* **66**:3667 (1977).
2. C. Ebner and W. F. Saam, *Phys. Rev. Lett.* **38**:1486 (1977).
3. M. R. Moldover and J. W. Cahn, *Science* **207**:1073 (1980).
4. R. Pandit, M. Schick, and M. Wortis, *Phys. Rev. B* **26**:5112; J. Fröhlich and C.-E. Pfister, *Europhys. Lett.* **3**:845 (1987), and references therein.
5. D. E. Sullivan, *Phys. Rev. B* **20**:3991 (1979); *J. Chem. Phys.* **74**:2604 (1981); E. Bruno, C. Caccamo, and P. Tarazona, *Phys. Rev. A* **35**:1218 (1987), and references therein.
6. M. R. Moldover and J. W. Schmidt, *Physica D* **12**:351 (1984).
7. M. Bienfait, J. L. Seguin, J. Suzanne, E. Lerner, J. Krim, and J. G. Dash, *Phys. Rev. B* **29**:983 (1984).
8. R. F. Kayser, M. R. Moldover, and J. W. Schmidt, *J. Chem. Soc. Faraday Trans. 2* **82**:1701 (1986).
9. M. P Nightingale and J. O. Indekeu, *Phys. Rev. B* **32**:3364 (1985).
10. J. O. Indekeu, *Phys. Rev. B* **36**:7296 (1987).
11. V. Privman, *J. Chem. Phys.* **81**:2463 (1984).

12. K. Abeysuriya, X.-L. Wu, and C. Franck, *Phys. Rev. B* **35**:6771 (1987); D. J. Durian, and C. Franck, *Phys. Rev. Lett.* **59**:555 (1987).
13. C. Ebner and W. F. Saam, *Phys. Rev. Lett.* **58**:587 (1987); *Phys. Rev. B* **35**:1822 (1987).
14. S. Dietrich, in *Phase Transitions and Critical Phenomena*, Vol. 12, C. Domb and J. Lebowitz, eds., to be published.
15. F. F. Abraham, *Adv. Phys.* **35**:1 (1986).
16. H. J. Herrmann, *Physica A* **140**:421 (1986).
17. J. H. Sikkenk, J. O. Indekeu, J. M. J. van Leeuwen, and E. O. Vossnack, *Phys. Rev. Lett.* **59**:98 (1987).
18. K. Binder, D. P. Landau, and D. M. Kroll, *J. Magn. Mat.* **54–57** 669 (1986).
19. G. Saville, *J. Chem. Soc. Faraday Trans. 2*, **73**:1122 (1977).
20. F. van Swol and J. R. Henderson, *J. Chem. Soc. Faraday Trans. 2* **82**:1685 (1988).
21. F. F. Abraham, *J. Chem. Phys.* **68**:3713 (1978).
22. A. F. Bakker, C. Bruin, F. van Dieren, and H. J. Hilhorst, *Phys. Lett.* **93A**:67 (1982); H. J. Hilhorst, A. F. Bakker, C. Bruin, A. Compagner, and A. Hoogland, *J. Stat. Phys.* **34**:987 (1984).
23. G. Navascues and M. V. Berry, *Mol. Phys.* **34**:649 (1977).
24. J. S. Rowlinson and B. Widom, *Molecular Theory of Capillarity* (Oxford University Press, 1982), p. 22.
25. R. Shuttleworth, *Proc. Phys. Soc. A* **63**:444 (1950).
26. H. Nakanishi and M. E. Fisher, *Phys. Rev. Lett.* **49**:1565 (1982).
27. M. Nijmeijer, J. H. Sikkenk, and C. Bruin, to be published.
28. M. E. Fisher, *J. Chem. Soc. Faraday Trans. 2* **82**:1828 (1985).
29. G. A. Chapela, G. Saville, S. M. Thompson, and J. S. Rowlinson, *J. Chem. Soc. Faraday Trans. 2* **8**:1133 (1977).
30. K. Kern, R. David, R. L. Palmer, and G. Comsa, *Phys. Rev. Lett.* **56**:2823 (1986).